Chapter 12
Stochastic Optimal Preventive Voltage Stability Control in Power Systems under Demand Response Program

Morteza Nojavan, Heresh Seyedi, and Behnam Mohammadi-Ivatloo

Nomenclature

α_b	Maximum percentage of demand-side participation in DR programs at bus b
β_b	Percentage of bus b load, which is no allowed to be shed
$\delta_b(s)$	Voltage angle at bus b for scenario s
$\delta_j(s)$	Voltage angle at bus j for scenario s
$\widetilde{\delta}_b(s)$	Voltage angle of bus b at loadability limit point for scenario s
$\widetilde{\delta}_j(s)$	Voltage angle of bus j at loadability limit point for scenario s
$\lambda(s)$	Loading parameter of the system for scenario s
$\lambda_{\text{thershold}}$	Satisfied loading parameter of the system
μi	Mean value of variable x_i
μj	Mean value of variable x_j
$\phi(\cdot)$	The *PDF* of standard normal function
ρ_{0ij}	A component in the correlation matrix ρ_0 of standard normal random vector Y
σi	Variance of the variable x_i
σj	Variance of the variable x_j
τ_{CC}	Lead time of preventive control
θbj	Angle of element b–j of the system Y_{bus} matrix
AD_i	Cost of reduction of active power generation of unit i (\$/MWh)
AI_i	Cost of increase in active power generation of unit i (\$/MWh)
B	Index of buses
CC_b^{DR}	Cost of DR participation at bus b
CC_b^{LS}	Cost of ILC at bus b

M. Nojavan (✉) · H. Seyedi · B. Mohammadi-Ivatloo
Faculty of Electrical and Computer Engineering, University of Tabriz, Tabriz, Iran
e-mail: m.nojavan@tabrizu.ac.ir; hseyedi@tabrizu.ac.ir; bmohammadi@tabrizu.ac.ir

S. Nojavan, K. Zare (eds.), *Demand Response Application in Smart Grids*,
https://doi.org/10.1007/978-3-030-32104-8_12

d	Index of load buses
$\mathrm{DRC}_b^p(s)$	Active part of DR program at bus b participating for scenario s
$\mathrm{DRC}_b^Q(s)$	Reactive part of DR program at bus b participating for scenario s
$f_{X_iX_j}(x_i, x_j)$	The joint *PDF* of random variables x_i, x_j
$F_i(x_i)$	The corresponding cumulative distribution function
G	Set of generating units
G_{F}	Set of fast-response generating units
$\mathrm{LS}_b^p(s)$	Active part of involuntary load curtailment (ILC) at bus b for scenario s
$\mathrm{LS}_b^Q(s)$	Reactive part of involuntary load curtailment (ILC) at bus b for scenario s
n	Number of PV buses in zone j
$P_{b,r}^{\mathrm{w}}$	Rated power of wind turbine installed at bus b
P_{G_i}	Active power generation of unit i
$P_{\mathrm{G}_i}^0$	Economic scheduled value of active power generation of unit i
$P_{\mathrm{G}_i}^-$	Active power reduction of generation unit i
$P_{\mathrm{G}_i}^+$	Increase in active power generation of unit i
$P_{\mathrm{G}_i}^{\min}$	Minimum active power generation of unit i
$P_{\mathrm{G}_i}^{\max}$	Maximum active power generation of unit i
$\widetilde{P}_{\mathrm{G}_i}(s)$	Active power generation of unit i at loadability limit point for scenario s
$P_{\mathrm{L}_b}(s)$	Active power load of bus b for scenario s
$Q_{\mathrm{G}_i}^0$	Economic scheduled value of reactive power generation of unit i
$Q_{\mathrm{G}_i}^{\min}$	Minimum reactive power generation of unit i
$Q_{\mathrm{G}_i}^{\max}$	Maximum reactive power generation of unit i
$Q_{\mathrm{G}_i}(s)$	Reactive power generation of unit i for scenario s
$\widetilde{Q}_{\mathrm{G}_i}(s)$	Reactive power generation of unit i at loadability limit point for scenario s
$Q_{\mathrm{G}_i}^+(s)$	Increase in reactive power generation of unit i for scenario s
$Q_{\mathrm{G}_i}^-(s)$	Decrease in reactive power generation of unit i for scenario s
$Q_{\mathrm{L}_b}(s)$	Reactive power load of bus b for scenario s
$\mathrm{RD}_{\mathrm{G}_i}$	Ramp-down rate of generating unit i
RD_i	Cost of reduction of reactive power generation of unit i (\$/MVarh)
RI_i	Cost of increase in reactive power generation of unit i (\$/MVarh)
$\mathrm{RU}_{\mathrm{G}_i}$	Ramp-up rate of generating unit i
s	Index for scenarios
S_{n}	Total number of scenarios
v	Wind speed
$v_{\mathrm{in}}^{\mathrm{c}}$	Cut-in speed of wind turbine
$v_{\mathrm{out}}^{\mathrm{c}}$	Cutoff speed of wind turbine
$v_{\mathrm{rated}}^{\mathrm{c}}$	Rated speed of wind turbine
$V_b(s)$	Magnitude of bus b voltage for scenario s

$V_j(s)$	Magnitude of bus j voltage for scenario s
$\widetilde{V}_b(s)$	Magnitude of bus b voltage at loadability limit point for scenario s
$V_b^{\min}$	Minimum voltage magnitude of bus b
$V_b^{\max}$	Maximum voltage magnitude of bus b
$\widetilde{V}_b^{\min}$	Minimum voltage magnitude of bus b at loadability limit point
$\widetilde{V}_b^{\max}$	Maximum voltage magnitude of bus b at loadability limit point
$\widetilde{V}_j(s)$	Magnitude of bus j voltage at loadability limit point for scenario s
$\lvert Y_{bj}\rvert$	Magnitude of b–jth element of the system Y_{bus} matrix

12.1 Introduction

Voltage stability refers to the ability of a power system to maintain steady voltages at all buses in the system after being subjected to a disturbance from a given initial operating condition [1]. One of the main reasons of various blackouts all over the world is voltage instability. Therefore, various studies have been executed and different methods have been proposed to identify and prevent voltage instability. Researches in this subject can be classified into two categories:

1. Voltage stability indices: the scope of this category is to present stability indices to identify voltage instability or determine the voltage stability margin.
2. Preventive and corrective control facilities to prevent voltage instability: this group includes researches about optimal preventive or corrective control actions to ensure desirable load margin.

Facilities used to prevent voltage instability in the preventive control schemes include load shedding, re-dispatch of active and reactive powers of generators, and demand response. Load shedding is one of the most important and also costly countermeasures against voltage instability. Various papers have proposed optimal under-voltage load shedding methods to ensure voltage stability with minimum involuntary load curtailment [2–9].

An optimal under-voltage load shedding methodology to avoid voltage instability is presented in [2]. The candidate buses for load shedding are selected based on the sensitivity of minimum eigenvalue of load flow Jacobian matrix with respect to the dropped load. The algorithm for minimum load shedding is developed using differential evolution. A centralized under-voltage load-shedding scheme considering the load characteristics is presented in [3]. In this research, dimensions of the optimal problem are greatly simplified using the proposed indicator. A practical approach for determining the best location and the minimum amount of load to be shed for voltage collapse prevention is presented in [4]. A multistage method is proposed to solve the problem. The main idea of the proposed method is to solve the optimization problem, stage by stage, and to limit the load shedding to a small amount at each stage. An adaptive under-voltage load-shedding scheme is proposed in [5] to protect

power system against voltage instability. Adaptive combinational load shedding methods are used to enhance power system stability in [6–9]. In the proposed algorithms, load shedding is started from the locations with higher voltage decay for longer period of time. The speed, location, and amount of load shedding are changed adaptively depending on the disturbance location, voltage status of the system, and the rate of frequency decline.

Load curtailment could be undesirable and too costly for the customers and consequently for the system operators. On the other hand, re-dispatch of active and reactive powers of generators and demand response programs can be used as facilities to maintain system voltage stability with lower costs. Papers in the second category have used the mentioned control facilities to prevent voltage collapse.

In [10, 11], a new method is presented for power system protection against voltage collapse based on the difference between apparent power flows at the sending and the receiving ends of the transmission lines. Then, a triggering signal is sent to the reactive power sources to increase reactive power production. Comprehensive control framework to ensure loading margin of power systems is proposed in [12]. Demand response, load shedding and rescheduling of generating units are control facilities in [12]. Online diagnosis of capacitor switching to prevent voltage collapse based on the measurement of actual load powers and voltages is presented in [13]. Reactive power rescheduling is used as a facility to improve voltage stability in [14]. Using ranking coefficients, the generators are divided into "important" and "less-important" ones. At the next step, voltage stability margin is improved by decreasing and increasing reactive power generation at the less-important and important generators, respectively.

Impact of uncertain input variables on the output parameters is one of the major requirements in the power system planning and operation. Load and wind power are the important uncertain parameters in power systems. Hence, the load and wind power uncertainties must be considered in power system analysis. Several research papers have considered load uncertainty and stochastic wind power generation modeling. Optimum sizing of a hybrid wind–photovoltaic–battery system is formulated in [15] considering wind speed, solar radiation, and electricity demand. Influence of using solar and wind forecast and their uncertainties on the optimization of demand response of the economic dispatch of an isolated microgrid system is analyzed in [16]. In [17] the optimal sizing of distributed generation in a hybrid power system with wind and energy storage units is presented considering load demand and wind speed uncertainties. Correlated wind power for probabilistic optimal power flow is presented in [18]. Point estimate method is used for solving probabilistic optimal power flow. Biogeography-based optimization algorithm with weighted sum method is proposed in [19] to solve probabilistic multi-objective optimal power flow problem. Nataf transformation based on traditional point estimate method is utilized to handle the correlation of wind sources and load demands. A powerful tool for quantifying the impact of DG units on active loss and voltage profile is proposed which considers the unbundling rules. A method to carry the uncertainty of wind speed for optimal stochastic economic dispatch problem is presented in [20]. An effective approach for deriving robust solutions to the

security-constrained unit commitment problem, considering load and wind power uncertainties, is presented in [21]. An optimization-based real-time residential load management algorithm considering load uncertainty in order to minimize the energy payment for each user is presented in [22]. The proposed algorithm just requires some statistical estimates of the future load demand. A new method for corrective voltage control considering wind power generation and demand values uncertainties is proposed in [23]. Objectives of the proposed method are to ensure a desired loading margin while minimizing the corresponding control cost. It is supposed that all loads and wind powers increase or decrease at the same time. Then, the proposed method uses a simple and somewhat unreal modeling of load and wind power uncertainties.

Wind power and load are the important uncertain parameters in power systems. These uncertainties and correlation among them should be considered in power system modeling, especially voltage instability prevention problems. For this reason in this chapter, a new preventive voltage instability problem is presented considering correlated uncertain wind power and load, preventive actions cost, the complete nonlinear model of the system and demand response. The effect of these uncertainties and their correlation on voltage instability prevention costs is evaluated using a new scenario-based approach. The main contribution of this chapter is correlated wind and load uncertainties modeling in voltage stability control for first time.

The remainder of this chapter is organized as follows: Section 12.2 presents uncertain correlated wind power and load scenario generation steps. Section 12.3 indicates preventive voltage instability problem formulation. Simulation results are presented in Sect. 12.4. Finally, discussions and conclusions are presented in Sect. 12.5.

12.2 Uncertainty Sources

Main uncertainty sources are load and wind power generation in this chapter. Modeling of the correlation of these uncertain sources is presented in this section.

12.2.1 Modeling of Correlated Uncertain Wind Power Generations

The wind turbine's powers have correlation based on weather conditions and location. Hence, the correlation of wind powers must be considered to model the actual condition and real estimation of preventive voltage instability actions cost.

In this section, the wind power scenario generation method is presented. Wind power generation is an uncertain parameter. This parameter can be modeled

probabilistically using historical data of wind speed [23]. Variation of wind speed is modeled using Rayleigh probability density function (PDF):

$$\mathrm{PDF}(v) = \left(\frac{2v}{c^2}\right) \exp\left(-\left(\frac{v}{c}\right)^2\right) \tag{12.1}$$

The generated power of a wind turbine in terms of wind speed is estimated as follows [23]:

$$P_b^{\mathrm{w}}(v) = \begin{cases} 0 & \text{if } v \le v_{\mathrm{in}}^{\mathrm{c}} \text{ or } v \ge v_{\mathrm{out}}^{\mathrm{c}} \\ \dfrac{v - v_{\mathrm{in}}^{\mathrm{c}}}{v_{\mathrm{rated}}^{\mathrm{c}} - v_{\mathrm{in}}^{\mathrm{c}}} P_{b,r}^{\mathrm{w}} & \text{if } v_{\mathrm{in}}^{\mathrm{c}} \le v \le v_{\mathrm{rated}} \\ P_{b,r}^{\mathrm{w}} & \text{else} \end{cases} \tag{12.2}$$

The Cholesky decomposition is used for generation of correlated uncertain wind power scenarios. This method is explained in details in [24]. The components of correlation matrix can be calculated as the following:

$$\begin{aligned} \rho_{ij} &= \int_{-\infty}^{+\infty} \int_{-\infty}^{+\infty} \left(\frac{x_i - \mu_i}{\sigma_i}\right)\left(\frac{x_j - \mu_j}{\sigma_j}\right) f_{X_i X_j}(x_i, x_j)\, dx_i dx_j \\ &= \int_{-\infty}^{+\infty} \int_{-\infty}^{+\infty} \left(\frac{F_i^{-1}(\phi(y_i)) - \mu_i}{\sigma_i}\right)\left(\frac{F_i^{-1}(\phi(y_i)) - \mu_j}{\sigma_j}\right) \\ &\quad \times \phi_2(y_i, y_j, \rho_{0ij})\, dy_i dy_j \end{aligned} \tag{12.3}$$

where

$$\phi_n(y, \rho_0) = \frac{1}{\sqrt{(2\pi)^n \det(\rho_0)}} \exp\left(-\frac{1}{2} y^{\mathrm{T}} \rho_0 y\right) \tag{12.4}$$

If ρ and the marginal PDFs are known, ρ_0 can be determined completely by solving nonlinear Eqs. (12.3) and (12.4). Then, Choleskey decomposition is applied to ρ_0 as the following:

$$\rho_0 = L_0 {L_0}^{\mathrm{T}} \tag{12.5}$$

L_0 is the lower triangular matrix in Eq. (12.5). Afterwards, the mutually independent standard normal random vector $\boldsymbol{U}$ can be calculated as follows:

$$\boldsymbol{U} = {L_0}^{-1} Y \tag{12.6}$$

Finally, the correlated scenarios can be calculated as the following:

$$S = \mu + \boldsymbol{U} \tag{12.7}$$

where S and μ are the correlated wind power scenarios and mean values of wind power, respectively.

12.2.2 Correlated Uncertain Load Scenario Generation

The method of load scenarios generation is presented in this section, considering load uncertainty and correlation among loads. The electrical distances between buses are calculated in the first step. Then, the power system is divided into several areas based on these distances. In the next step, load correlation matrix is defined according to the identified zones. Finally, uncertain correlated load scenarios are generated based on the correlation matrix.

12.2.2.1 Electrical Distance Calculation

Electrical distance calculation is presented in details in [25]. The step-by-step method to obtain the electrical distance between two buses is given in the following:

1. The Jacobian matrix J is calculated and the submatrix $J_4 = [\partial Q/\partial V]$ is obtained.
2. J_4 ($B = J_4^{-1}$) is inverted. The elements of matrix B are written as $b_{ij} = \partial V_i/\partial Q_j$.
3. Attenuation matrix between all buses is calculated using the following equation:

$$\alpha_{ij} = b_{ij}/b_{jj} \tag{12.8}$$

4. Electrical distances, D_{ij}, between ith and jth buses are calculated:

$$D_{ij} = -\log\left(\alpha_{ij}.\alpha_{ji}\right) \tag{12.9}$$

5. The electrical distances are normalized as follows:

$$D_{ij} = D_{ij}/\mathrm{Max}(D_{i1}, \ldots, D_{iN}) \tag{12.10}$$

Partitioning of power system is presented in Sect. 12.2.2.2, based on these normalized electrical distances.

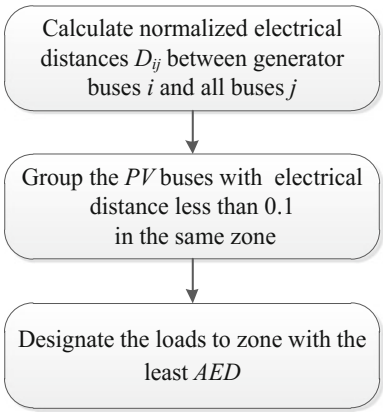

Fig. 12.1 Partitioning of power system

12.2.2.2 Partitioning of Power System

The normalized electrical distances D_{ij} between generator buses i and all other buses j are calculated according to descriptions presented in Sect. 12.2.1. Then, the PV buses are grouped in different zones as shown in the flow chart of Fig. 12.1. In this figure, the average of electrical distance for load i in zone j (AED_{ij}) is calculated as follows:

$$\text{AED}_{ij} = \frac{\sum_{k=1}^{n} D_{ik}}{n} \tag{12.11}$$

12.2.2.3 Generation of Correlation Matrix and Scenarios

In general, the loads in one zone are more influenced by common causes such as common weather or similar power-consuming behavior in comparison to the loads in other zones. Then, the correlation among loads in one zone is stronger than that of other zones. As a result, based on the above assumptions and the assumptions of [26], the correlation coefficients between loads are as follows:

- The correlation coefficients between loads at the same zone are assumed to be 0.8.
- The correlation coefficients between loads at neighboring zones are assumed to be 0.4.
- The correlation coefficients between loads at different zones are assumed to be 0.1.

The correlated load scenarios are generated based on the correlation matrix and Eqs. (12.3)–(12.7).

12.3 Preventing Voltage Instability Problem Formulation

The load margin is indicated by a simple *P–V* curve of bus. The load margin is defined as the distance between the system-operating point and voltage collapse point. This margin is shown in Fig. 12.2. In this figure, λ, B, and A are load margin, the system-operating point, and voltage collapse point, respectively. The load margin is indicated in details in [12].

In order to achieve the desired load margin, the generated active and reactive powers of power plants could either be decreased or increased. In the case of power decrease, opportunity cost should be paid, but in the case of power increase, electricity cost should be paid to the participant power plants. Figure 12.3 indicates this method. Considering this figure, $P^0_{G_i}$ is the economic scheduled generation, while $AI_i P_{Gi}{}^+$ and $AD_i{}^- P_{Gi}{}^-$ are costs, which should be paid to the units in case of increase or decrease with respect to their economic scheduled active power generation, respectively.

Demand response programs are presented in details in [12]. Direct load control (DLC) and interruptible/curtailable (I/C) programs are used in this chapter as different terms of objective function.

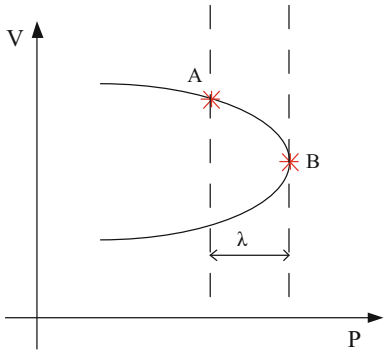

Fig. 12.2 The bus's *P–V* curve

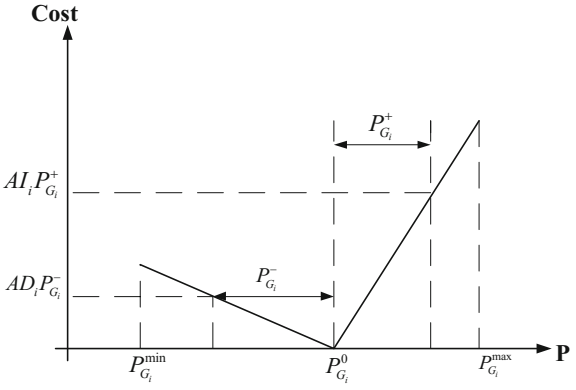

Fig. 12.3 The rule of paying cost to generators

Load shedding is considered as the last and most expensive control facility to prevent voltage instability. Hence, this facility is considered as the highest price term in the objective function.

The proposed facilities are classified into two different categories based on [23]. These categories are named here-and-now and wait-and-see. The values of wait-and-see facilities differ from one scenario to another, while values of here-and-now facilities are the same for all scenarios. Demand response, load shedding, and reactive power outputs of power plants are proposed as wait-and-see facilities, while active power outputs of power plants are proposed as here-and-now facilities [23].

Objective function of the proposed problem is presented as follows:

$$F = \sum_{i\in \mathrm{G_F}} \left(\mathrm{AD_i} P^{-}_{\mathrm{G}_i} + \mathrm{AI}_i P^{+}_{\mathrm{G}_i} \right) + \sum_{s=1}^{S_n} \left(\sum_{i\in \mathrm{G_F}} \left(\mathrm{RD}_i Q^{-}_{\mathrm{G}_i}(s) + \mathrm{RI}_i Q^{+}_{\mathrm{G_i}}(s) \right) \right.$$

$$\left. + \sum_{b\in d} \left(\mathrm{CC}^{\mathrm{DR}}_b \mathrm{DRC}^{p}_b(s) + \mathrm{CC}^{\mathrm{LS}}_b \mathrm{LS}^{p}_b(s) \right) \right) \Big/ S_n \tag{12.12}$$

This objective function contains the cost of preventive control facilities (generator active and reactive re-dispatch, load shedding, and demand response).

Considered constraints are formulated as the following:

$$\begin{aligned} &\sum_{i\in \mathrm{G_F}} P_{\mathrm{G}_i} - \left(P_{\mathrm{L}_b}(s) - \mathrm{DRC}^{p}_b(s) - \mathrm{LS}^{p}_b(s) \right) \\ &= \sum_{j\in B} V_b(s) V_j(s) \left| Y_{bj} \right| \cos\left(\delta_b(s) - \delta_j(s) - \theta_{bj} \right) \quad \forall b \in B \end{aligned} \tag{12.13}$$

$$\begin{aligned} &\sum_{i\in G} Q_{\mathrm{G}_i} - \left(Q_{\mathrm{L}_b}(s) - \mathrm{DRC}^{Q}_b(s) - \mathrm{LS}^{Q}_b(s) \right) \\ &= \sum_{j\in B} V_b(s) V_j(s) \left| Y_{bj} \right| \sin\left(\delta_b(s) - \delta_j(s) - \theta_{bj} \right) \quad \forall b \in B \end{aligned} \tag{12.14}$$

$$\mathrm{DRC}^{Q}_b(s) = 0.75 * \mathrm{DRC}^{p}_b(s) \quad \forall b \in B \tag{12.15}$$

$$\mathrm{LS}^{Q}_b(s) = 0.75 * \mathrm{LS}^{p}_b(s) \quad \forall b \in B \tag{12.16}$$

$$V^{\min}_b \le V_b(s) \le V^{\max}_b \tag{12.17}$$

$$0 \le P^{+}_{\mathrm{G}_i} \le \mathrm{RU}_{\mathrm{G}_i} \times \tau_{\mathrm{CC}} \quad i \in G_{\mathrm{F}} \tag{12.18}$$

$$0 \le P^{-}_{\mathrm{G}_i} \le \mathrm{RD}_{\mathrm{G}_i} \times \tau_{\mathrm{CC}} \quad i \in G_{\mathrm{F}} \tag{12.19}$$

$$P_{\mathrm{G}_i} = P^{0}_{\mathrm{G}_i} + P^{+}_{\mathrm{G}_i} - P^{-}_{\mathrm{G}_i} \quad i \in G_{\mathrm{F}} \tag{12.20}$$

$$P^{\min}_{\mathrm{G}_i} \le P_{\mathrm{G}_i} \le P^{\max}_{\mathrm{G}_i} \quad i \in G_{\mathrm{F}} \tag{12.21}$$

$$Q_{\mathrm{G}_i}(s) = Q^0_{\mathrm{G}_i} + Q^+_{\mathrm{G}_i}(s) - Q^-_{\mathrm{G}_i}(s) \quad i \in G \tag{12.22}$$

$$Q^{\min}_{\mathrm{G}_i} \le Q_{\mathrm{G}_i}(s) \le Q^{\max}_{\mathrm{G}_i} \quad i \in G \tag{12.23}$$

$$\begin{aligned}&\sum_{i\in G}\widetilde{P}_{\mathrm{G}_i} - \left(P_{\mathrm{L}_b}(s) - \mathrm{DRC}^p_b(s) - \mathrm{LS}^p_b(s)\right)(1+\lambda(s))\\ &= \sum_{j\in B}\widetilde{V}_b(s)\widetilde{V}_j(s)\left|Y_{bj}\right|\cos\left(\widetilde{\delta}_b(s) - \widetilde{\delta}_j(s) - \theta_{bj}\right) \quad \forall b \in B\end{aligned} \tag{12.24}$$

$$\begin{aligned}&\sum_{i\in G}\widetilde{Q}_{\mathrm{G}_i}(s) - \left(Q_{\mathrm{L}_b}(s) - \mathrm{DRC}^Q_b(s) - \mathrm{LS}^Q_b(s)\right)(1+\lambda(s))\\ &= \sum_{j\in B}\widetilde{V}_b(s)\widetilde{V}_j(s)\left|Y_{bj}\right|\sin\left(\widetilde{\delta}_b(s) - \widetilde{\delta}_j(s) - \theta_{bj}\right) \quad \forall b \in B\end{aligned} \tag{12.25}$$

$$\lambda(s) > \lambda_{\text{thershold}} \tag{12.26}$$

$$0 \le \mathrm{DRC}^P_b(s) \le \alpha_b P_{\mathrm{L}_b}(s) \tag{12.27}$$

$$0 \le \mathrm{DRC}^Q_b(s) \le \alpha_b Q_{\mathrm{L}_b}(s) \tag{12.28}$$

$$0 \le \mathrm{LS}^P_b(s) \le (1-\alpha_b-\beta_b)P_{\mathrm{L}_b}(s) \tag{12.29}$$

$$0 \le \mathrm{LS}^Q_b(s) \le (1-\alpha_b-\beta_b)Q_{\mathrm{L}_b}(s) \tag{12.30}$$

$$\widetilde{V}^{\min}_b \le \widetilde{V}_b(s) \le \widetilde{V}^{\max}_b \tag{12.31}$$

The power balance equations for active and reactive power are presented by (12.13) and (12.14). Equations (12.15) and (12.16) present constant power factor for necessary under-voltage load shedding and demand response. Bus voltage limit is indicated by (12.17). Equations (12.18) and (12.19) indicate ramp up and ramp down of power plants. Eqs. (12.21) and (12.23) state the capacity limit of the generators. Satisfied load margin is expressed by (12.26). Eqs. (12.27)–(12.30) indicate limitation of demand response and curtailed load of each bus. Equations (12.24), (12.25), and (12.31) are constraints for voltage collapse point.

12.4 Simulation Results

The proposed method is simulated on the large scale IEEE 118-bus test system. The costs of re-dispatching active and reactive powers of generating units AD_i, AI_i, RD_i, and RI_i are assumed to be 125, 25, 12.5, and 2.5% of the base-case locational marginal price (LMP) of buses connected to the generating units, respectively. The costs of load shedding and demand response at each bus are considered to be 100 and 10 times of LMP of that bus, respectively [12]. 150-MW turbines are connected at nodes17, 30, 59, 80, 92, and 100 [18]. The correlation is equal to 0.88 among the turbine pairs (17, 30), (59, 80), and (92,100) and is set to 0.48 for others [18].

Table 12.1 Grouping of generator buses

Group 1	G1(B1),G2(B4),G3(B6),G4(B8),G5(B10),G6(B12)
Group 2	G7(B15),G8(B18),G9(B19),G53(B113)
Group 3	G10(B24),G11(B25),G12(B26),G32(B72)
Group 4	G13(B27),G14(B31),G15(B32)
Group 5	G16(B34),G17(B36),G18(B40),G19(B42),G20(B46),G21(B49),G22(B54),G23 (B55),G24(B56),G25(B59),G26(B61),G27(B62),G28(B65),G29(B66),G30(B69), G54(B116)
Group 6	G31(B70),G33(B73),G34(B74)
Group 7	G35(B76),G36(B77),G37(B80)
Group 8	G38(B85),G39(B87),G40(B89),G41(B90),G42(B91),G43(B92)
Group 9	G44(B99),G45(B100),G46(B103),G47(B104),G48(B105),G49(B107), G50(B110), G51(B111),G52(B112)

The proposed algorithm is simulated in GAMS and MATLAB environments. The scenarios are generated in MATLAB environment, and voltage instability prevention problem is solved in GAMS software using NLP method.

12.4.1 Partitioning of the System

The IEEE 118-bus test system consists of 54 generating units and 186 transmission lines. The system data are presented in [12]. The proposed method for partitioning the system is applied to the IEEE 118-bus test system. This test system is divided into nine zones based on the algorithm presented in Fig. 12.1. Table 12.1 presents generators of each group. In this table, G7 (B15) means generator number 7 in bus number 15 as an example. Figure 12.4 shows different zones of the mentioned test system.

12.4.2 Scenario Generation and Analysis

Three cases are studied in this section as described in the following:

Case 1: Preventive voltage instability problem is solved under load and wind power generation uncertainties based on the method of references [23, 27] as a simple and unreal condition. Table 12.2 shows generated scenarios in this case.

Case 2: Preventive voltage instability problem is solved under uncorrelated load and wind power generation uncertainties for 20 scenarios.

Case 3: Preventive voltage instability problem which is assumed as a real condition is solved under correlated load and wind power generation uncertainties for 20 scenarios.

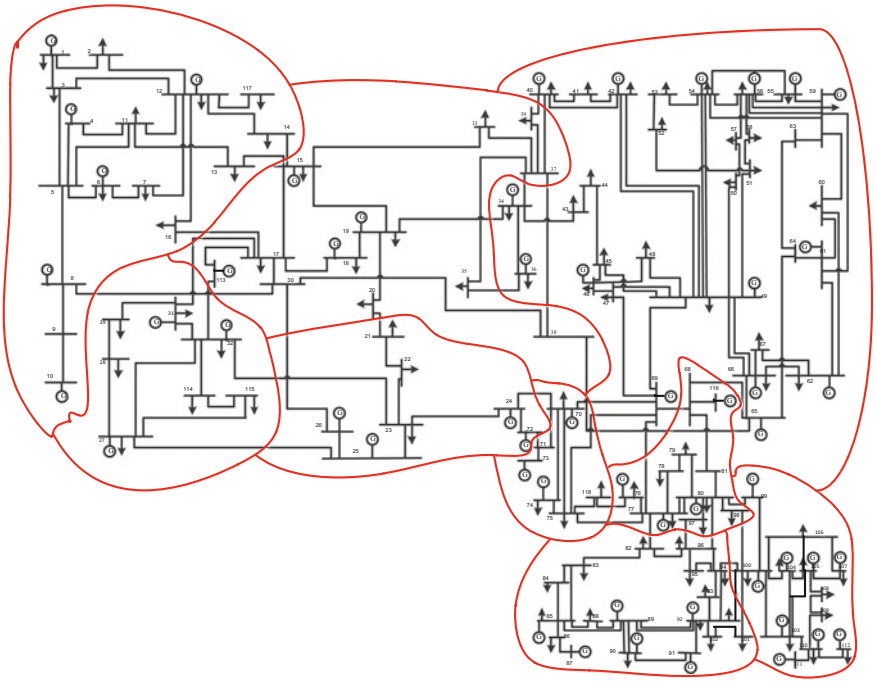

Fig. 12.4 Different zones of IEEE 118-bus test system

Table 12.2 Wind-load scenarios in Case 1

Scenario number	Load (%)	Wind (%)
S1	98	100
S2	100	100
S3	102	100
S4	98	50
S5	100	50
S6	102	50
S7	98	0
S8	100	0
S9	102	0

The number of proposed scenarios for wind power and loads are 4 and 5 in Cases 2 and 3, respectively. Hence, total 20 wind-load correlated scenarios are generated in this section based on the explanations provided in Sect. 12.2.

The total wind power scenarios and total load scenarios are shown in Figs. 12.5 and 12.6 for Cases 1, 2, and 3, respectively. Considering these figures, total load variation in Case 3 is greater than that of Case 2.

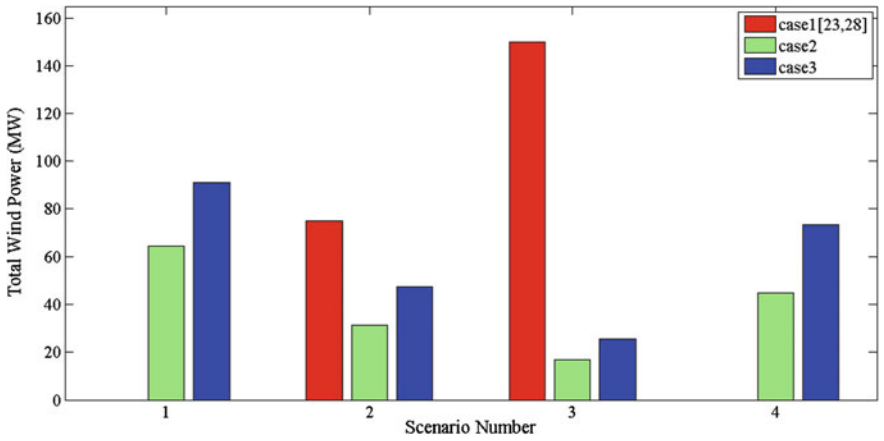

Fig. 12.5 Total wind power for each scenario in Cases 1, 2, and 3

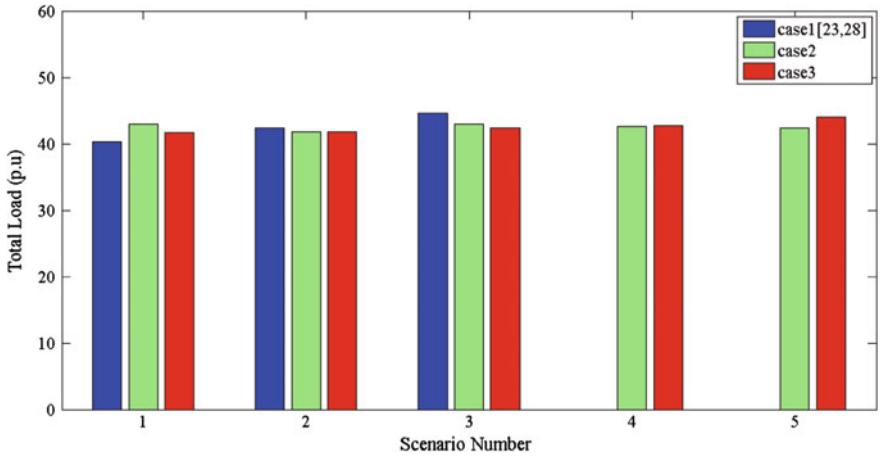

Fig. 12.6 Total load for each scenario in Cases 1, 2, and 3

The value of objective function is $4427.1 for Case 1. In this case, load shedding is not necessary. The value of demand response for nine scenarios is shown in Table 12.3 for Case 1. Objective function for 20 scenarios is $4896.4 for Case 2. Load shedding is not necessary in the 20 proposed scenarios. The value of demand response for 20 scenarios is shown in Table 12.4 for Case 2. In Case 3, objective function for 20 scenarios is $8178.7. In this case, load shedding is not necessary. The value of demand response for 20 scenarios is shown in Table 12.5 for Case 3.

The value of demand response for 9 scenarios in Case 1 and for 20 scenarios in Cases 2 and 3 are compared in Fig. 12.7. Considering this figure, for most scenarios, the value of demand response in Case 3 is greater than the value of demand response

Table 12.3 Values of demand response for 9 scenarios in Case 1

Scenario number	Demand response (p.u.)
1	0
2	0
3	0.7948
4	0
5	0
6	0.7766
7	0
8	0
9	0.7585

Table 12.4 Values of demand response for 20 scenarios in Case 2

Scenario number	Demand response (p.u.)	Scenario number	Demand response (p.u.)
1	0	11	0.062
2	0	12	0
3	0.0937	13	0.2846
4	0	14	0
5	0	15	0
6	0	16	0
7	0	17	0
8	0.1654	18	0
9	0	19	0
10	0	20	0

Table 12.5 Values of demand response for 20 scenarios in Case 3

Scenario number	Demand response (p.u.)	Scenario number	Demand response (p.u.)
1	0	11	0.1418
2	0	12	0
3	0	13	0
4	0	14	0
5	1.6424	15	1.7924
6	0.0822	16	0
7	0	17	0
8	0	18	0
9	0	19	0
10	1.7334	20	1.5844

in Cases 1 and 2. As a result, objective function in Case 3, as a real case, is greater than that in Cases 1 and 2.

Actual system loads and wind powers have correlation based on weather conditions and location. Hence, the correlation among loads and wind powers must be

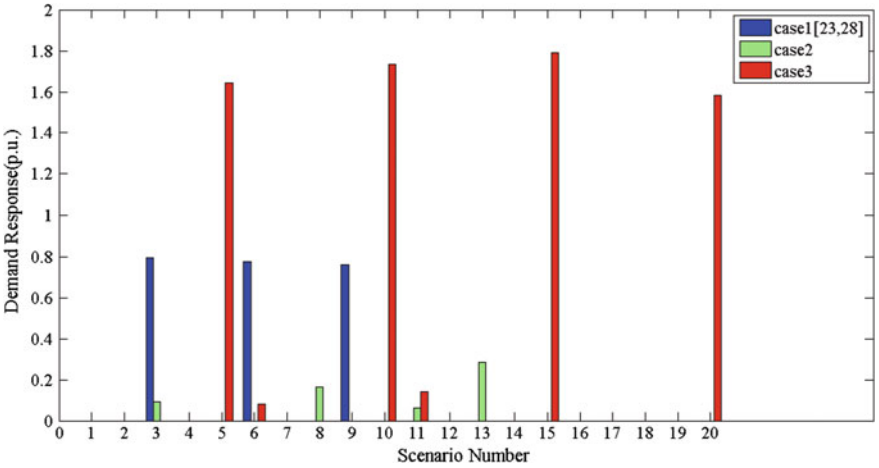

Fig. 12.7 Demand response value in Cases 1, 2, and 3

Table 12.6 Summary of the simulation results

	Total demand response (p.u.)	Objective function($)
Case 1 [23, 27]	2.328	4427.1
Case 2	0.6057	4896.4
Case 3	6.9766	8178.7

considered to model the actual condition. Considering these correlations, the cost of preventive actions is increased, based on the results of simulations. Therefore, if these correlations are not considered, the cost of preventive actions is underestimated. This fact illustrates the necessity of accurate load and wind power modeling in voltage stability evaluation.

12.4.3 Summary of Simulation Results

In this section, the simulation results are summarized to illustrate the necessity of correlation modeling. The results are presented in Table 12.6. According to Table 12.6, a noticeable difference in values of total demand response and objective function in Case 3 indicates the necessity of correlated load and wind power modeling in preventive voltage instability problem.

12.5 Conclusion

A new stochastic optimal preventive voltage stability control is presented in this chapter under correlated wind power and load uncertainties. Correlation matrix for wind turbine and loads are defined based on electrical distance and partitioning of the power system. Then, scenarios are generated and voltage instability prevention problem is solved. The control facilities in the proposed problem are classified into two categories. They are named here-and-now and wait-and-see. A new algorithm is presented to simulate real condition of power system. The proposed method is tested on the 118-bus IEEE standard test system. The system is simulated for three cases: wind and load uncertainties modeling based on previous research works, uncorrelated wind and load uncertainties, and correlated wind and load uncertainties. Case 3 is assumed close to the actual condition due to correlation among wind turbine powers and loads in real power systems. The analysis indicates higher cost of preventive actions for real conditions. In other words, to obtain realistic results for the cost of voltage instability prevention, both uncertainty and correlation among wind turbines powers and loads must be considered, according to the proposed method of this chapter.

References

1. IEEE/CIGRE Joint Task Force on Stability Terms & Definitions, ed. by P. Kundur (2002)
2. L.D. Arya, P. Singh, L.S. Titare, Differential evolution applied for anticipatory load shedding with voltage stability considerations. Int. J. Electr. Power Energy Syst. **42**(1), 644–652 (2012)
3. J. Deng, J. Liu, A study on a centralized under-voltage load shedding scheme considering the load characteristics, in *International Conference on Applied Physics and Industrial Engineering* (2012), pp. 481–489
4. Y. Wang, I.R. Pordanjani, W. Li, W. Xu, E. Vaahedi, Strategy to minimise the load shedding amount for voltage collapse prevention. IET Gener. Transm. Distrib. **5**(3), 307–313 (2011)
5. T. Amraee, A.M. Ranjbar, R. Feuillet, Adaptive under-voltage load shedding scheme using model predictive control. Electr. Power Syst. Res. **81**(7), 1507–1513 (2011)
6. A. Saffarian, M. Sanaye-Pasand, Enhancement of power system stability using adaptive combinational load shedding methods. IEEE Trans. Power Syst. **26**(3), 1010–1020 (2011)
7. H. Seyedi, M. Sanaye-Pasand, New centralized adaptive load-shedding algorithms to mitigate power system blackouts. IET Gener. Transm. Distrib. **3**(1), 99–114 (2009)
8. H. Seyedi, M. Sanaye-Pasand, Design of new load shedding special protection schemes for a double area power system. Am. J. Appl. Sci. **6**(2), 317–327 (2009)
9. M. Sanaye-Pasand, H. Seyedi, Centralized adaptive load shedding methods to enhance power system voltage stability margins. IEEJ Trans. Electr. Electron. Eng. **3**(6), 669–679 (2008)
10. G. Verbic, F. Gubina, A new concept of protection against voltage collapse based on local phasors, in *International Conference on Power System Technology* (2000), pp. 965–970
11. I. Šmon, M. Pantoš, F. Gubina, An improved voltage-collapse protection algorithm based on local phasors. Electr. Power Syst. Res. **78**(3), 434–440 (2008)
12. A. Rabiee, M. Parvania, M. Vanouni, M. Parniani, M. Fotuhi-Firuzabad, Comprehensive control framework for ensuring loading margin of power systems considering demand-side participation. IET Gener. Transm. Distrib. **6**(12), 1189–1201 (2012)

13. F. Karbalaei, M. Kalantar, A. Kazemi, On line diagnosis of capacitor switching effect to prevent voltage collapse. Energy Convers. Manag. **51**(11), 2374–2382 (2010)
14. H. Raoufi, M. Kalantar, Reactive power rescheduling with generator ranking for voltage stability improvement. Energy Convers. Manag. **50**(4), 1129–1135 (2009)
15. A. Maleki, M. Gholipour Khajeh, M. Ameri, Optimal sizing of a grid independent hybrid renewable energy system incorporating resource uncertainty and load uncertainty. Int. J. Electr. Power Energy Syst. **83**, 514–524 (2016)
16. D. Neves, M.C. Brito, C.A. Silva, Impact of solar and wind forecast uncertainties on demand response of isolated microgrids. Renew. Energy **87**(2), 1003–1015 (2016)
17. A.M. Abd-el-Motaleb, S. Kazem Bekdach, Optimal sizing of distributed generation considering uncertainties in a hybrid power system. Int. J. Electr. Power Energy Syst. **82**, 179–188 (2016)
18. C.S. Saunders, Point estimate method addressing correlated wind power for probabilistic optimal power flow. IEEE Trans. Power Syst. **29**(3), 1045–1054 (2014)
19. S. Shargh, B.K. Ghazani, B. Mohammadi-ivatloo, H. Seyedi, M. Abapour, Probabilistic multi-objective optimal power flow considering correlated wind power and load uncertainties. Renew. Energy **94**(1), 10–21 (2016)
20. A.H. Shahirinia, E.S. Soofi, D.C. Yu, Probability distributions of outputs of stochastic economic dispatch. Int. J. Electr. Power Energy Syst. **81**, 308–316 (2016)
21. B. Hu, W. Lei, M. Marwali, On the robust solution to SCUC with load and wind uncertainty correlations. IEEE Trans. Power Syst. **29**(6), 2952–2964 (2014)
22. P. Samadi, H. Mohsenian-Rad, W.W. Vincent, R. Schober, Tackling the load uncertainty challenges for energy consumption scheduling in smart grid. IEEE Trans. Smart Grid **4**(2), 1007–1016 (2013)
23. A. Rabiee, A. Soroudi, B. Mohammadi-Ivatloo, M. Parniani, Corrective voltage control scheme considering demand response and stochastic wind power. IEEE Trans. Power Syst. **29**(6), 2965–2973 (2014)
24. H. Li, L. ZhenZhou, X. Yuan, Nataf transformation based point estimate method. Chin. Sci. Bull. **53**(17), 2586–2592 (2008)
25. J. Zhong, E. Nobile, A. Bose, K. Bhattacharya, Localized reactive power markets using the concept of voltage control areas. IEEE Trans. Power Syst. **19**(3), 1555–1561 (2004)
26. W. Li, R. Billinton, Effect of bus load uncertainty and correlation in composite system adequacy evaluation. IEEE Trans. Power Syst. **6**(4), 1522–1529 (1991)
27. S.M. Mohseni-Bonab, A. Rabiee, B. Mohammadi-ivatloo, Voltage stability constrained multi-objective optimal reactive power dispatch under load and wind power uncertainties: a stochastic approach. Renew. Energy **85**(1), 598–609 (2016)